

A Free-Boundary Model of Diffusive Valley Growth: Theory and Observation

Robert Yi¹, Yossi Cohen¹, Hansjörg Seybold¹, Eric Stansifer¹, Robb McDonald², Mark Mineev-Weinstein³, and Daniel H. Rothman¹

¹*Lorenz Center, Department of Earth, Atmospheric, and Planetary Sciences, Massachusetts Institute of Technology, Cambridge, MA*

²*Department of Mathematics, University College London, London, UK*

³*International Institute of Physics, Federal University of Rio Grande do Norte, Natal, Brazil*

June 14, 2017

Abstract

Valleys that form around a stream head often develop characteristic finger-like elevation contours. We study the processes involved in the formation of these valleys and introduce a theoretical model that indicates how shape may inform the underlying processes. We consider valley growth as the advance of a moving boundary travelling forward purely through linearly diffusive erosion, and obtain a solution for the valley shape in three dimensions. Our solution compares well to the shape of slowly growing groundwater-fed valleys found in Bristol, Florida. Our results identify a new feature in the formation of groundwater-fed valleys: a spatially variable diffusivity that can be modelled by a fixed-height moving boundary.

Keywords: Moving boundary problem, valley growth, erosion

1 Introduction

Flowing water carves beautiful, diverse features into landscapes [1]. The mechanism by which it does so is fundamentally simple: water accumulates and flows downstream, forming rivers with the capacity to transport soil and rocks and erode these landscapes [2]. Depending on the properties of the surface being eroded, different physical processes influence this erosion and consequently leave behind diverse topographic signatures. In particular, when the eroded sediment originates from the topography in the vicinity of the river, its transport downstream facilitates the formation of valleys by imposing a boundary condition to which the topography is subject. For landscapes whose surfaces are sufficiently shallow and composed of homogeneous soil rather than rock, the evolution of the surface is approximately linearly diffusive [3, 4, 5]. When this sediment is transported downstream at a rate that exceeds the rate at which it is supplied, these rivers can be considered as fixed-height absorbing boundaries of diffusive topography [6]. The quasistatic topographic response to

this forcing is what we call a valley, and we seek to understand the form of these valleys in what follows.

Two models describing the formation of soil-mantled valleys can be found in recent works, and both compare valley formation to other well-studied diffusive systems. Pelletier and Perron [7] find that the parabolic isotherms predicted for a solidifying front in a temperature field [8] agree well with the topographic contours of storm-eroded valleys in Southern Arizona, where water flows over the surface of the topography. Petroff et al. [9] find that isolated contours of groundwater-fed valleys in Bristol, Florida are similar to the steady-state shape of the interface formed when a less viscous fluid is injected between glass plates containing a more viscous fluid [10]. Both results suggest that these valleys are similar to an interface moving through a diffusive field, but because their boundary conditions differ, so too do the resulting shapes of the valley they predict.

To explore this issue, we construct a theory for valleys that diffuse around nearly stationary streams. We hypothesize that, when the streams are fed by groundwater, such valleys exhibit a height-dependent diffusivity. In an asymptotic limit, this variable diffusivity can be approximated as a fixed-height moving boundary at the rim of the valley, or *valley edge*. We introduce a free-boundary model that incorporates this element: linear diffusion of topography within an expanding valley edge of specified height. This model predicts a valley shape, which we compare both to real valleys and shapes predicted by the previously mentioned models of valley formation. This appears to be the first time that a real two-dimensional elevation field (that is, a contour map) is compared to a predicted valley shape. Our results demonstrate how physical features can be incorporated into models of valley growth as boundary conditions. By exploring this connection, we shed light on how shape can reveal the mechanisms involved in the history of valley growth.

2 The Physical Picture

We consider a model in which valleys form as surface topography diffuses into an absorbing stream. Rainsplash, vegetation growth and death, freeze-thaw cycles, and animal burrowing are the primary mechanisms that produce topographic diffusion, known as soil creep [4, 11]. In the continuum limit, soil creep has been observed to follow a Fickian law at shallow slopes [3, 12]:

$$q = -D\nabla H, \tag{1}$$

where H is topographic height, D is a diffusivity with units m^2/s , and q is volumetric flux per unit width. In other words, the rate at which soil travels downslope is proportional to the steepness of that slope.

2.1 The Moving Boundary

We hypothesize that the presence of groundwater renders the diffusivity D height-dependent. Because the upland region of groundwater-fed valleys is further from the water table than the sloped region within the valley, the region outside the valley is drier than within the valley. The relatively flat upland also receives more insolation, amplifying the effect. Depending on

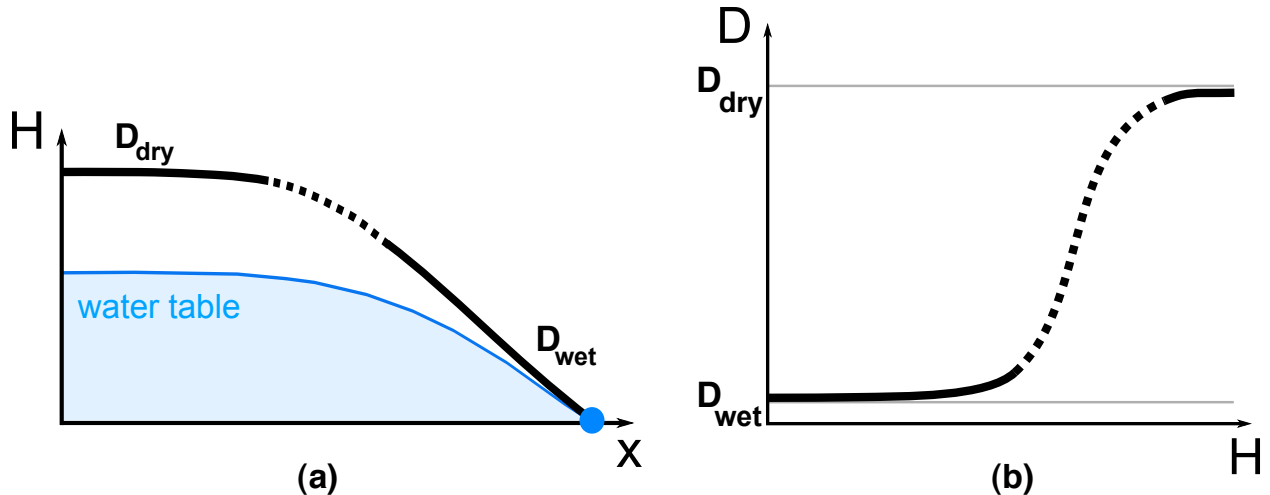


Figure 1: Schematic illustration of the variability of diffusivity with height H . (a) A vertical cross-section through a valley with diffusivities D_{wet} at small H and D_{dry} at large H . The transitional region is indicated by the dotted line. The location of the stream is indicated by the dot on the x axis. (b) The function $D(H)$, which we assume varies rapidly near the valley edge. The transitional region is again indicated by the dotted line.

climate, vegetation may also enhance it. The relative dryness outside the valley increases the diffusivity [13, 14, 6], producing a height-dependent diffusivity as illustrated in Figure 1.

Taking D_{wet} to be the lower bound of the diffusivity close to the water table and D_{dry} to be the upper bound of diffusivity outside the valley, we consider the limit in which $D_{\text{wet}}/D_{\text{dry}} \rightarrow 0$. In this limit, the upland topography diffuses infinitely quickly compared to the valley, and so we take the height of the upland region to be constant. In the limit where the transitional region is thin, diffusivity is a step function at a critical height H_0 . Figure 2 shows how these approximations appear for a real valley.

This description resembles other models of moving boundaries in diffusive fields. For example, when a fluid of low viscosity slowly displaces a fluid of higher viscosity, the velocity of the two fluids must be the same on each side of the interface. The smaller viscosity of the invading fluid then requires that pressure gradients within the invading fluid be small compared to the defender. The relatively uniform pressure within the invader then translates to a constant-pressure boundary condition at the interface [10].

3 Mathematical Representation

We now formalize these components into a single moving-boundary problem. By construction, our theory will model only the late stages of valley growth, where the valley edge moves much faster than the spring advances, the memory of the initial conditions has almost vanished, and we approach a characteristic shape.

Consider a valley of topographic height $H(x, y, t)$ growing around a stream γ at height $H = 0$, which flows along a path from $x = 0$ to $x \rightarrow -\infty$ along $y = 0$, as shown in Figure 3. We write the valley edge as $\Gamma(t)$, on which $H = H_0 = \text{const.} > 0$. Let $\Omega(t)$ be

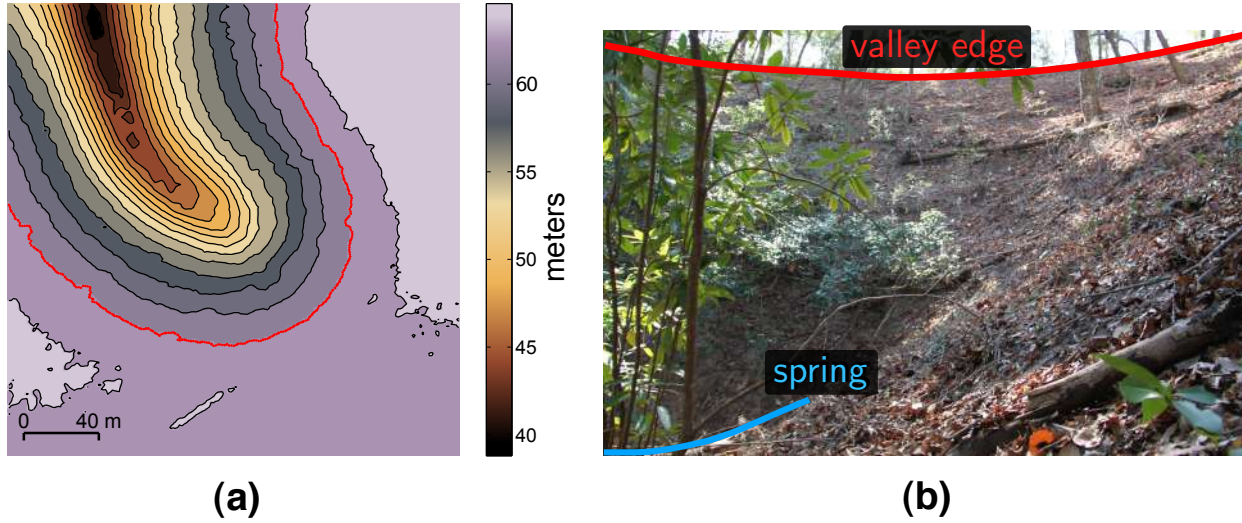


Figure 2: (a) A topographic map of the valley in Figure 7a. Elevation is measured with respect to NAVD 88. The valley edge roughly corresponds to the red contour. (b) An oblique view of the interior of a real valley.

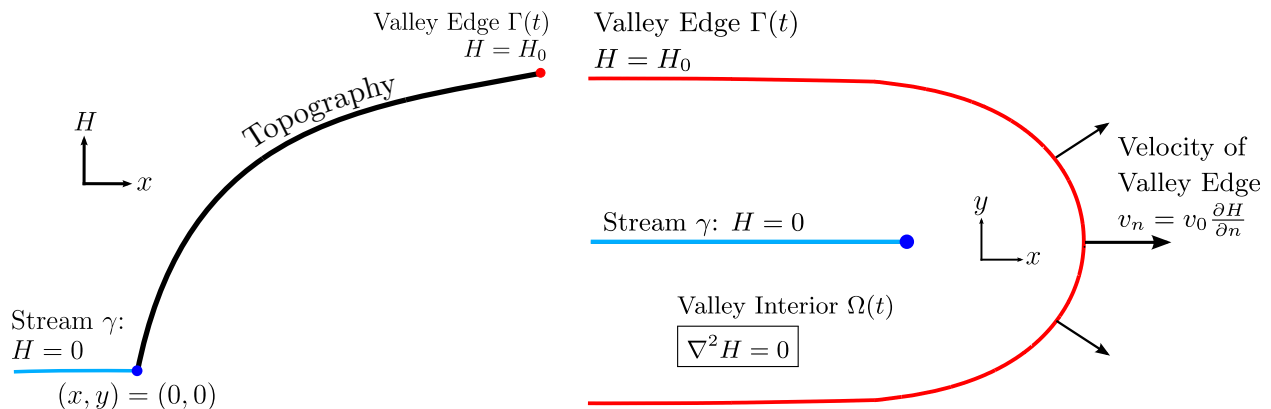


Figure 3: Illustration of diffusive valley growth. Left: side-view. Right: planform, top-down view.

the region between γ and $\Gamma(t)$. We assume that the topographic elevation, $H(x, y, t)$, is diffusive in Ω , and that the normal velocity v_n of the valley edge Γ is linearly proportional to the normal derivative of H at this edge. This velocity condition assumes that sediment flux is proportional to slope. For a very slow rate of valley growth, the time derivative in the diffusion equation can be neglected. In this quasistatic limit, our system of equations is

$$\begin{aligned}
 H &= 0 && \text{on } \gamma \\
 H &= H_0 && \text{on } \Gamma(t) \\
 v_n &= v_0 \frac{\partial H}{\partial n} && \text{on } \Gamma(t) \\
 \nabla^2 H &= 0 && \text{in } \Omega(t).
 \end{aligned} \tag{2}$$

We nondimensionalize distance and time, setting $h = H/H_0$, $x \rightarrow x/H_0$, $y \rightarrow y/H_0$, and

$t \rightarrow v_0 t / H_0$. The system of equations becomes

$$\begin{aligned}
h &= 0 && \text{on } \gamma \\
h &= 1 && \text{on } \Gamma(t) \\
v_n &= \frac{\partial h}{\partial n} && \text{on } \Gamma(t) \\
\nabla^2 h &= 0 && \text{in } \Omega(t).
\end{aligned} \tag{3}$$

The solution to this problem satisfies a kind of shape invariance, namely

$$h(r^\alpha x, r^\alpha y, rt) = h(x, y, t), \tag{4}$$

which is to say that the valley grows outwards as time increases. A shape invariant solution will necessarily satisfy the initial condition $\Gamma(0) = \gamma$. In fact, we will find that $\alpha = \frac{1}{2}$ as would be expected for a diffusive process.

To see this, we consider the behaviour of h for large, negative values of x far away from the stream tip $(x, y) = (0, 0)$. From the boundary conditions, we expect that any oscillations or perturbations in Γ to be damped out with time. Because γ is stationary, h should become independent of x for large, negative x , so $\frac{\partial h}{\partial x} = 0$. Then, because $\nabla^2 h = 0$ in Ω , we have $\frac{\partial^2 h}{\partial y^2} = 0$, so h is a linear function of y from $y = 0$ to the boundary $y = L(t)$, where L is the limiting half-width of Ω as $x \rightarrow -\infty$. This has the linear solution $h(x, y, t) = |y| / L$. From the boundary condition we have $\frac{dL}{dt} = v_n = \left| \frac{\partial h}{\partial y} \right| = \frac{1}{L}$ on the boundary $y = \pm L$, giving $L = \sqrt{2t}$.

Now that we know the shape of Ω in the limit as $x \rightarrow -\infty$, we solve for the full shape. We conformally map Ω to the upper-half plane, which is possible by the Riemann mapping theorem. This allows us to solve Laplace's equation $\nabla^2 h = 0$ in the upper-half plane and then transform it back to our original coordinate system, as Laplace's equation remains unchanged by conformal maps. At this point it becomes useful to use complex coordinates $z = x + iy$ to describe Ω and h . We seek a map from z to $\zeta = \xi + i\eta$ which sends Ω to the upper-half plane $\eta > 0$, Γ to the interval $\eta = 0, -1 < \xi < 1$, and γ to the two intervals $\eta = 0, |\xi| > 1$. The upper edge of γ goes to $\xi > 1$ and the lower edge goes to $\xi < 1$. An illustration of this map is shown in Figure 4. The required map is found in Appendix A and is given by

$$\frac{z}{\sqrt{2t}} = \frac{2}{\pi} + \frac{\zeta}{\pi} \log \left(\frac{\zeta - 1}{\zeta + 1} \right). \tag{5}$$

Now working in the ζ -plane, we can find $h(\zeta)$ as a solution to Laplace's equation $\nabla^2 h = 0$ in the region $\eta > 0$ with the boundary conditions that $h = 1$ on the interval $\eta = 0, -1 < \xi < 1$ and $h = 0$ on the two intervals $\eta = 0, |\xi| > 1$. Particularly since h is a function of ζ alone and does not vary in time in the ζ -plane, this forces h to satisfy the shape invariance discussed above. We write h as the imaginary part of a function $\omega = \phi + ih$, which is analytic on the upper-half plane. The relation

$$\omega = \frac{1}{\pi} \log \left(\frac{\zeta - 1}{\zeta + 1} \right) \tag{6}$$

satisfies these conditions.

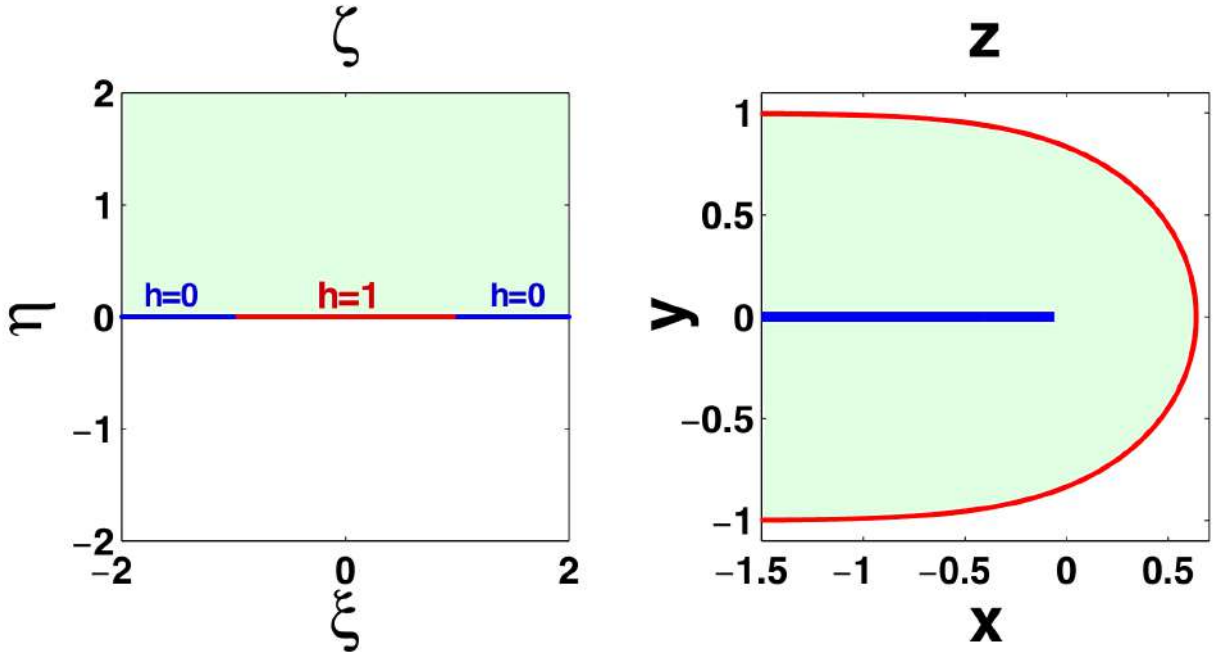


Figure 4: An illustration of the conformal map from the physical coordinates $z = x + iy$ to the mathematical coordinates $\zeta = \xi + i\eta$. The blue line in both plots indicates the stream γ , the red line indicates the valley edge Γ , and the light green region indicates the domain Ω .

Combining equations (5) and (6) we can relate z to ω through

$$\frac{z}{\sqrt{2t}} = \frac{2}{\pi} - \omega \coth \frac{\pi\omega}{2}. \quad (7)$$

Taking the imaginary part of ω as a function of z lets us recover the height h as a function of x and y . In particular, restricting to $h = 1$ yields a relationship between x and y on the boundary $\Gamma(t)$:

$$x = \frac{2}{\pi}\sqrt{2t} + \frac{y}{\pi} \log \left(\frac{\sqrt{2t} - y}{\sqrt{2t} + y} \right). \quad (8)$$

A 3D perspective view of the full solution is shown in Figure 5. For convenience, we henceforth refer to our model as the *Fickian finger* model, so named for the linear dependence of soil creep on slope reminiscent of Fick's first law of diffusion and the finger-like shape of the valley edge.

4 Selection of Slow-growing Valleys

To test our mathematical formulation, we compare the Fickian finger model to valleys within a network of groundwater-fed streams in Bristol, Florida. Valleys in this area are composed primarily of homogeneous, unconsolidated quartz sand [15, 16].

Our model focuses on a slow-growing regime where diffusive relaxation is linear and the stream head does not advance. Consequently, selected valleys must have shallow slopes to

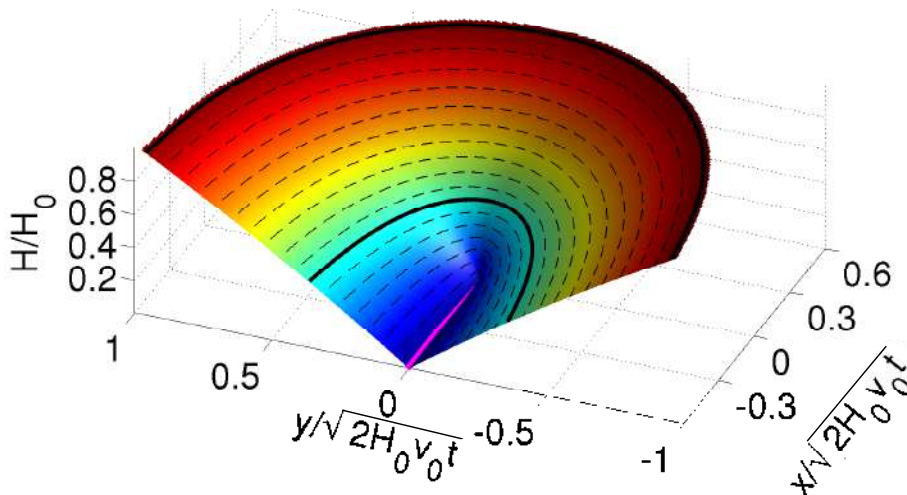


Figure 5: Solution to Equation (2). The straight magenta line indicates the location of the stream. The bold contour is at $H_0/3$.

be slow-growing and maintain linear transport. Moreover, they should be isolated from other valleys to reduce the influence of non-local effects. Practically, we seek two properties associated with these criteria: we seek to minimize the proportion of each valley with slopes steeper than the angle of repose, and we seek to maximize distance to the nearest downstream branch.

To find fraction of the valley area that is at or above the critical slope, we use a flow accumulation model [17] to determine contributing topographic areas to each stream head, then find regions whose slopes are greater than 0.5, or 26.6° . This is a loose threshold for the angle of repose, which is generally higher than 30° for dry grains [18]. We determine the length of channels by calculating the arclength along extracted streams from stream tips to the nearest downstream junction. We find a linear trend with the proportion of area above the angle of repose, shown in Figure 6. This suggests that valleys with longer streams are diffusively dominated, and we find several valleys which fall at the end of this trend, indicated by red circles in Figure 6. These valleys can be characterized as long, unbranched, and gently sloped.

5 Comparison to Field Data

We now proceed to compare valleys A-E in Figure 6 to our model. For each valley, topographic relief was obtained through laser altimetry data with a horizontal resolution of 1.2 m and a vertical resolution of about 5 cm [19]. The valley was then rotated in the horizontal plane such that the first twenty meters of stream from the stream head were aligned with the stream of the theoretical valley. We then fit 5 parameters (three coordinates for the position of the channel head, one scale factor for topographic height, and one scale factor for valley width and length) to minimize the least-squares difference between the elevations of the two surfaces.

We find that the upper two-thirds of valleys specified in Figure 6 agree well with our

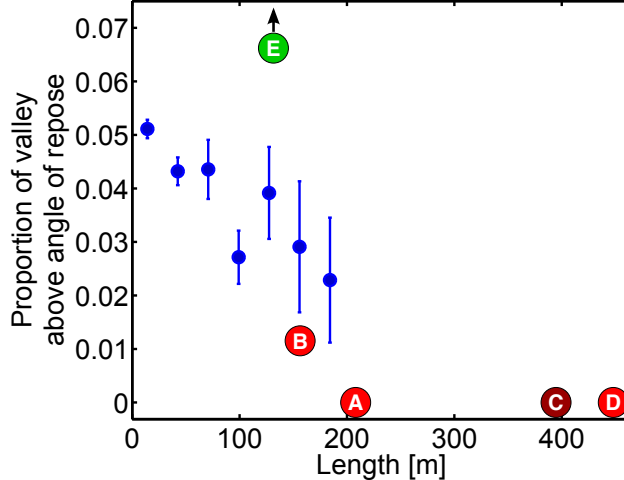


Figure 6: The fraction of the valley (extracted by the flow accumulation algorithm of Tarboton [17]) that is above the angle of repose as a function of channel length. The fitted valleys in Figure 7, shown here in red, fall at the end of this trend – long and largely below the threshold of motion. Valley E (green) is a poorly-fitting head, shown in Figure 9. The arrow above valley E indicates that the actual proportion of valley E above the angle of repose is 0.17. See Appendix B for further discussion.

theoretical shape, shown in Figure 7. This agreement suggests that large regions of these valleys behave diffusively within the boundaries of the constant-height valley edge predicted by the theory. Appendix B presents the contexts of these valleys within the network.

These valleys fit poorly within the bottom third of the valley (the region inside the bold contour in Figures 5 and 7). We attribute the poor fit in this region to an inability of the topography to sustain the infinite slope at the stream head associated with the $h \sim \sqrt{x}$ headward profile (see Appendix C). Figure 8 exposes this problem. An alternative boundary condition could be an interior absorbing contour that surrounds the singular river and represents the valley floodplain (a region that is flooded during storms, and thus may intermittently act as an absorbing boundary), as proposed by Pelletier and Perron [7]. If we constrain an interior contour of our solution such that its growth scales with the size of the valley and stays at a height $h = 0$, we find, however, that our problem becomes overspecified. The solution to this free boundary problem is the same as that which we solved earlier, and the shape of the interior boundary is a chosen contour of our present solution. The solution around an infinitely thin needle-shaped boundary, therefore, fully represents our class of solutions. However, solutions around a contour that does not scale linearly with the size of the valley may produce different results.

We also compare our solution to a valley with higher sediment flux (marked in green in Figure 6), as shown in Figure 9. We find that it fits poorly by comparison, supporting our premise that the Fickian finger model best approximates end-member, slow-moving valleys.

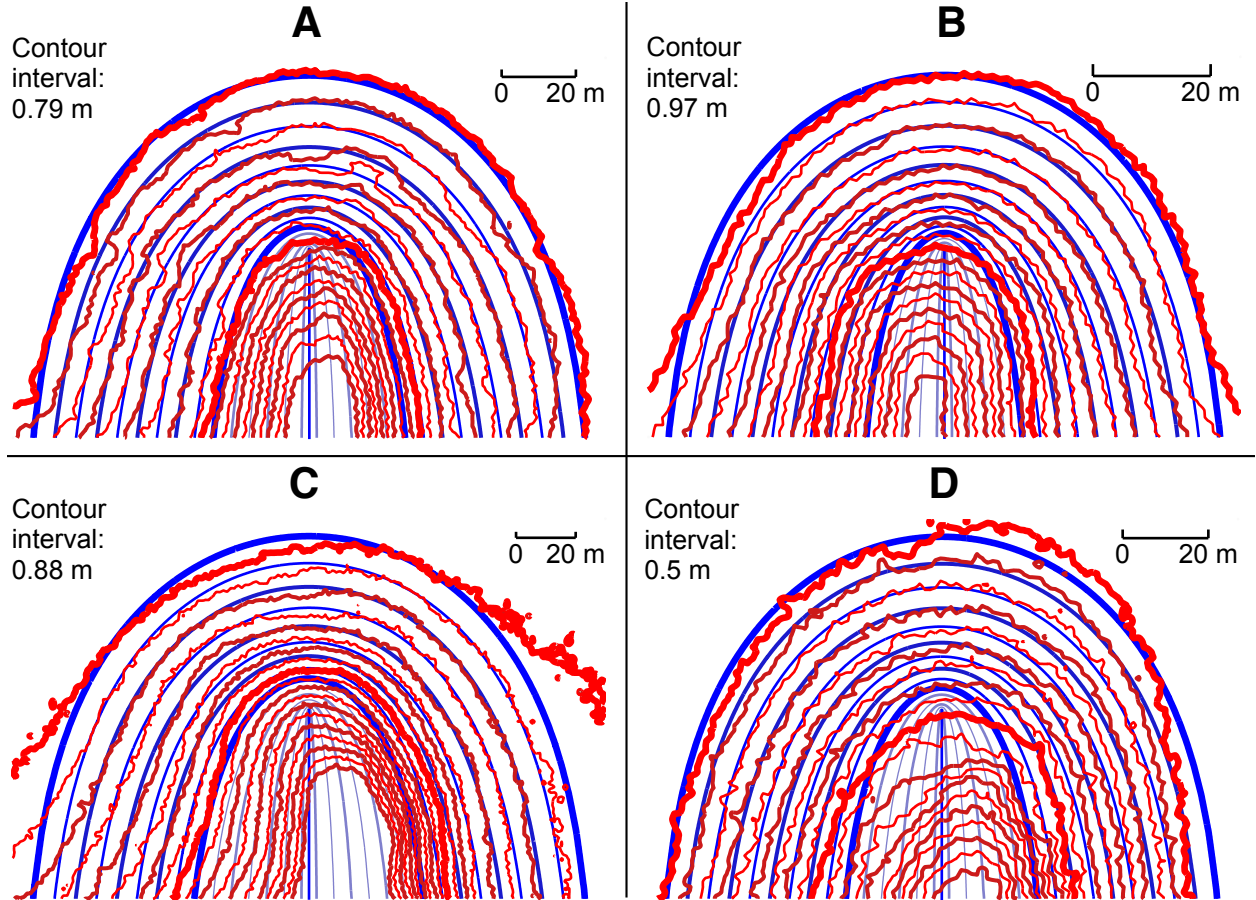


Figure 7: Fits of our model to several slow-growing valleys. The bold interior contour is at $H_0/3$. The outermost contour shown in A is the red contour indicated in Figure 2.

6 Comparison to Other Models

6.1 Ivantsov Parabolic Front [7]

Pelletier and Perron [7] give the only previous theoretical model for a valley growing in three dimensions, using the solution of Ivantsov [8] for the temperature field around a crystalline needle. Their model solves a steady-state diffusion equation in a moving reference frame:

$$\begin{aligned}
 H &= 0 && \text{in } \gamma_p \\
 H &= H_\infty && \text{as } x \rightarrow \infty \text{ and } y \rightarrow \pm\infty \\
 -v_s \frac{dH}{dy} &= \kappa \nabla^2 H
 \end{aligned} \tag{9}$$

where γ_p indicates the valley floor, or floodplain, bounded by a parabola $x \sim -y^2$, H_∞ is the asymptotic height of the topography in the upland, κ is a diffusivity, and v_s is the velocity of the stream tip.

Figure 10 shows that this model fits poorly to the valley head in Figure 7(a). This misfit results from physical differences between the models: the Pelletier and Perron [7] solution

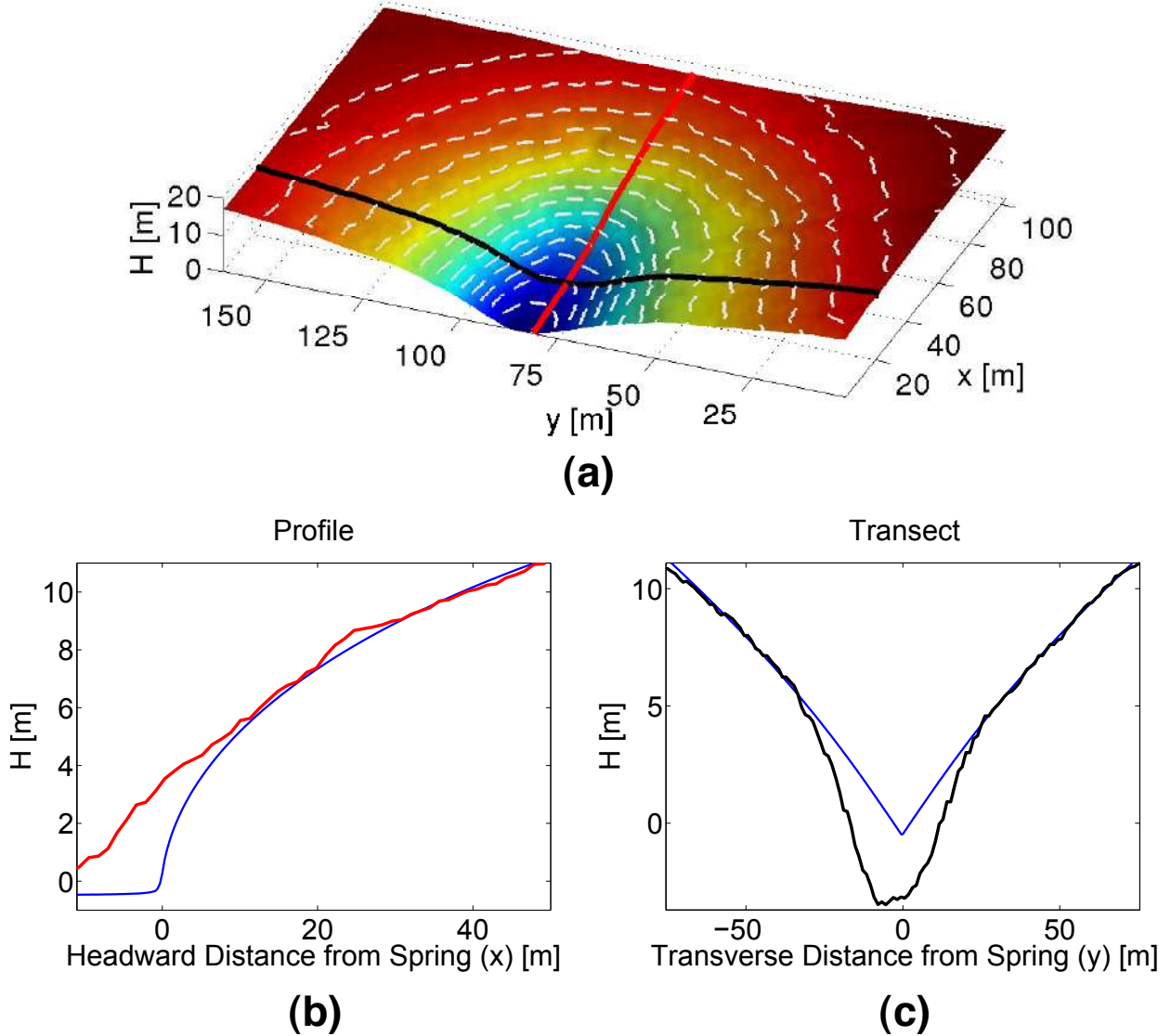


Figure 8: (a) A perspective plot of the valley in Figure 7a. The headward valley relief (b) and the valley relief perpendicular to the direction of growth 30 meters downstream from the extracted spring (c) for the valley in Figure 7a are shown in red and black, respectively. The theoretical profile and transect are shown in blue. The misfit near the stream reflects the inability of landscapes to sustain the infinite slope of the $H \sim \sqrt{x}$ profile predicted by our theory.

describes a steady-state form as diffusion balances the advance of the stream head, while the Fickian finger model describes relaxation around a stationary stream.

A distinguishing feature of the Pelletier-Perron model is that the contours are unbounded in y as $x \rightarrow -\infty$, which result from the advance of the stream head. In their model, the topography downstream of an advancing stream head has had a longer time to diffuse than topography in the vicinity of the stream head, so the valley grows wider downstream. On the other hand, bounded contours would indicate that the stream head is moving forward

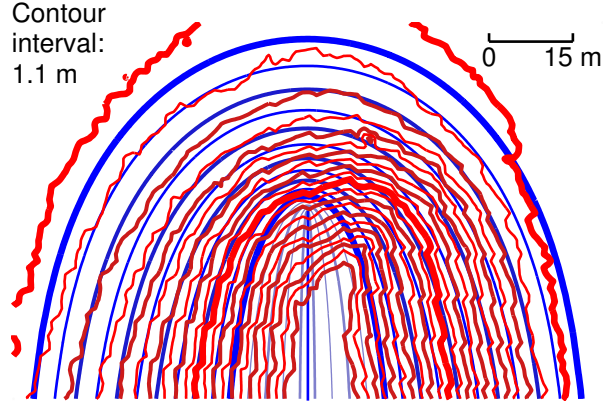


Figure 9: An example of a poorly fitting valley (valley ‘E’ in Figure 6). Contour lines of the topographic relief are fit to and superimposed over contours of the Fickian finger model. Appendix B presents the context of this valley within the network.

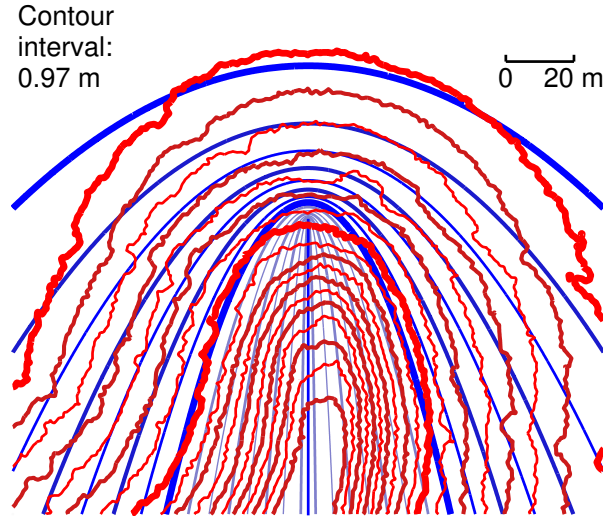


Figure 10: The valley of Figure 7(a) fit to the Pelletier and Perron [7] model.

at a negligible velocity. The absence or presence of bounded contours can therefore reveal whether or not the stream head is advancing.

6.2 Curvature-Driven Growth [9]

The shape of the valley edge predicted by our theory bears remarkable similarity to the contour shape predicted by Petroff et al. [9]. Our theory predicts the shape

$$x = \frac{2l}{\pi} + \frac{y}{\pi} \log \left(\frac{l-y}{l+y} \right), \quad (10)$$

which originates from the conformal map in Equation (5). Petroff et al. [9] predict a contour of the form

$$x = \frac{2l}{\pi} + \frac{2l}{\pi} \log \cos \left(\frac{\pi y}{2l} \right), \quad (11)$$

identical to the Saffman-Taylor finger [10], which Petroff et al. [9] obtain from an assumption of curvature-driven growth. A notable difference between (10) and (11) is the aspect ratio set by the product $2l\kappa$, where κ is the curvature of the contour at $y = 0$ and l is the asymptotic half-width of the contour as $x \rightarrow -\infty$. For the Fickian finger valley edge, this product is $8/\pi \approx 2.55$, while for the contour of Petroff et al. [9], this product is π [9]. A comparison between the contours predicted by the two theories is shown in Figure 11(a).

Aside from the fact that the Fickian finger model incorporates a third dimension (the height of the diffusive field) that the Petroff et al. [9] model does not, the shape difference can be attributed to the different growth laws on the moving boundary. The valley edge of the Fickian finger grows at a velocity $v_n = v_0 \frac{dH}{dn}$, while the model of Petroff et al. [9] grows at a rate proportional to the local curvature.

7 Conclusion

We have tested the hypothesis that topographic relaxation can be described simply as linear diffusion of topographic height within a constant-height, expanding boundary. We find agreement of real valleys to the shape predicted by this theory, providing us with strong, novel evidence for both linear diffusion as a responsible mechanism and an elevation-dependent diffusivity in groundwater-fed valleys. In particular, our results reveal a separation of timescales between the wet valley and the dry upland that produces an interface along which we can prescribe a constant height and diffusive rate of growth. Moreover, through comparison of the Fickian finger model to other models of valley growth, we deduce that bounded, “finger-like” contours suggest that the stream head within a valley is either not advancing or advancing slowly. Our results suggest that the shape of a valley can inform our understanding of the physical processes that generate these shapes. Further study of other end-member valleys may yet reveal other properties that impart their own unique topographic signatures on the geometry of valley growth.

Data, code and materials

The datasets supporting this article have been uploaded as part of the supplementary material.

Competing interests

We have no competing interests.

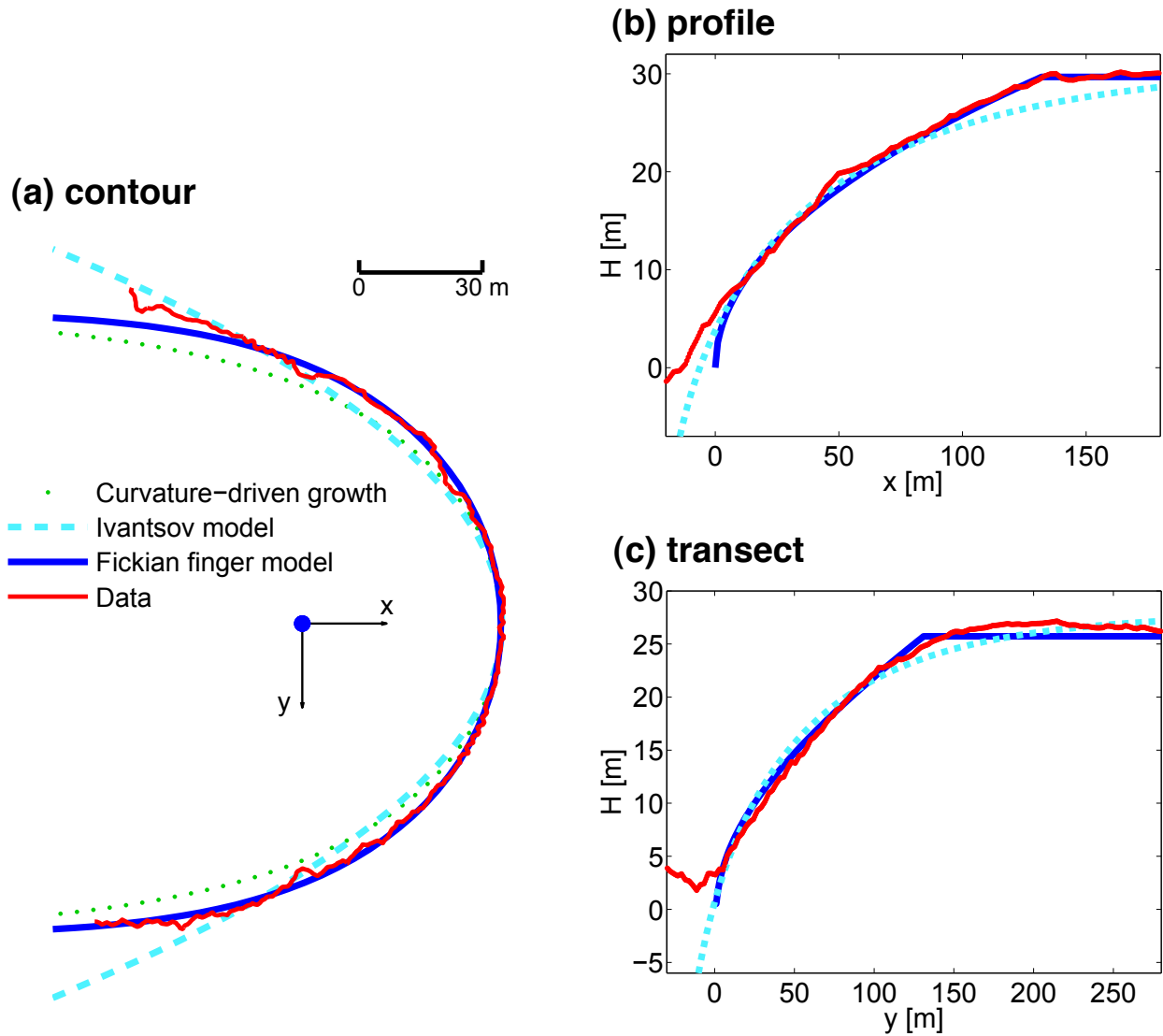


Figure 11: A shape comparison for three different valley shape theories. Features of the Fickian finger model are shown in blue, the log-cos contour of Petroff et al. [9] is shown in dotted green, features of the Ivantsov solution are shown in dashed cyan, and data from the valley in Figure 7(a) is shown in red. The blue dot in (a) indicates the location of (0, 0) in the Fickian finger model.

Authors' contributions

RSY, YC, HS, RM, MMW, and DHR designed research. RM and MMW derived the free boundary model. All authors contributed to the model's physical interpretation. RSY, HS, and DHR analysed data. RSY wrote the paper with contributions from ES, RM, MMW, and DHR. All authors gave final approval for publication.

Acknowledgements

This work was inspired by valleys from the Apalachicola Bluffs and Ravines Preserve in Bristol, Florida. We thank K. Flournoy, D. Printiss, A. Schmidt, J. Stites and the Nature Conservancy for access to and guidance within the Preserve. We also thank O. Devauchelle for his insightful comments.

Funding

This material is based upon work supported by the U.S. Department of Energy, Office of Science, Office of Basic Energy Sciences, Chemical Sciences, Geosciences, and Biosciences Division under Award Number FG02-99ER15004.

References

- [1] P.R. Bierman and D.R. Montgomery. *Key Concepts in Geomorphology*. W.H. Freeman, 2013.
- [2] D.F. Ritter, R.C. Kochel, and J.R. Miller. *Process Geomorphology*. Waveland Press, Inc., 2011.
- [3] W.E.H. Culling. Analytical theory of erosion. *The Journal of Geology*, pages 336–344, 1960.
- [4] W.E.H. Culling. Soil creep and the development of hillside slopes. *The Journal of Geology*, pages 127–161, 1963.
- [5] A.M. Heimsath, D.J. Furbish, and W.E. Dietrich. The illusion of diffusion: Field evidence for depth-dependent sediment transport. *Geology*, 33(12):949–952, 2005.
- [6] A.P. Petroff, O. Devauchelle, A. Kudrolli, and D.H. Rothman. Four remarks on the growth of channel networks. *Comptes Rendus Geoscience*, 344(1):33–40, 2012.
- [7] J.D. Pelletier and J.T. Perron. Analytic solution for the morphology of a soil-mantled valley undergoing steady headward growth: Validation using case studies in southeastern Arizona. *Journal of Geophysical Research: Earth Surface*, 117(F2), 2012.
- [8] G.P. Ivantsov. The temperature field around a spherical, cylindrical, or pointed crystal growing in a cooling solution. In *Dokl. Akad. Nauk SSSR*, volume 58, pages 567–569, 1947.
- [9] A.P. Petroff, O. Devauchelle, D.M. Abrams, A.E. Lobkovsky, A. Kudrolli, and D.H. Rothman. Geometry of valley growth. *Journal of Fluid Mechanics*, 673:245–254, 2011.
- [10] P.G. Saffman and G. Taylor. The penetration of a fluid into a porous medium or Hele-Shaw cell containing a more viscous liquid. In *Proceedings of the Royal Society of London*

- A: Mathematical, Physical and Engineering Sciences*, volume 245, pages 312–329. The Royal Society, 1958.
- [11] W.E.H. Culling. Theory of erosion on soil-covered slopes. *The Journal of Geology*, 73(2):230–254, 1965.
 - [12] W.E. Dietrich, D.G. Bellugi, L.S. Sklar, J.D. Stock, A.M. Heimsath, and J.J. Roering. Geomorphic transport laws for predicting landscape form and dynamics. *Prediction in geomorphology*, pages 103–132, 2003.
 - [13] S. Herminghaus. Dynamics of wet granular matter. *Advances in Physics*, 54(3):221–261, 2005.
 - [14] J.J. Roering. Soil creep and convex-upward velocity profiles: Theoretical and experimental investigation of disturbance-driven sediment transport on hillslopes. *Earth Surface Processes and Landforms*, 29(13):1597–1612, 2004.
 - [15] S.A. Schumm, K.F. Boyd, C.G. Wolff, and W.J. Spitz. A ground-water sapping landscape in the Florida panhandle. *Geomorphology*, 12(4):281–297, 1995.
 - [16] D.M. Abrams, A.E. Lobkovsky, A.P. Petroff, K.M. Straub, B. McElroy, D.C. Mohrig, A. Kudrolli, and D.H. Rothman. Growth laws for channel networks incised by ground-water flow. *Nature Geoscience*, 2(3):193–196, 2009.
 - [17] D.G. Tarboton. A new method for the determination of flow directions and upslope areas in grid digital elevation models. *Water resources research*, 33(2):309–319, 1997.
 - [18] S. Nowak, A. Samadani, and A. Kudrolli. Maximum angle of stability of a wet granular pile. *Nature Physics*, 1(1):50–52, 2005.
 - [19] O. Devauchelle, A.P. Petroff, H.F. Seybold, and D.H. Rothman. Ramification of stream networks. pages 2–6, 2012. doi: 10.1073/pnas.1215218109.
 - [20] S.D. Howison. Complex variables in industrial mathematics. In *Proceedings of the Second European Symposium on Mathematics in Industry*, pages 153–166. Springer, 1988.
 - [21] S.D. Howison and J.R. King. Explicit solutions to six free-boundary problems in fluid flow and diffusion. *IMA Journal of Applied Mathematics*, 42(2):155–175, 1989.
 - [22] L.J. Cummings, S.D. Howison, and J.R. King. Two-dimensional stokes and hele-shaw flows with free surfaces. *European Journal of Applied Mathematics*, 10(06):635–680, 1999.
 - [23] P. Polubarinova-Kochina. Theory of ground water movement. *Princeton University Press*, 1962.

A The Conformal Map

The map $z = f(\zeta)$ from the upper half of the ζ -plane to Ω is such that $\Gamma(t)$ maps to $\eta = 0$, $|\xi| < 1$, and γ to $\eta = 0$, $|\xi| > 1$, where the rays $\xi > 1$ and $\xi < -1$ map to the upper and lower edges of the stream, γ , respectively. The points $\zeta = \pm 1$ map to $z = \infty$ and the ‘strip’-like structure of width $\sqrt{8t}$ as $z \rightarrow \infty$ suggests that the map has the form

$$\frac{z}{\sqrt{2t}} = C + \frac{g(\zeta)}{\pi} \log \left(\frac{\zeta - 1}{\zeta + 1} \right), \quad (12)$$

where $g(\zeta)$ is some analytic function of ζ , which will be found below, and C is a constant. The valley symmetry and the oddness of the logarithm in (12) with respect to ζ demands that $g(\zeta)$ be an odd function of ζ and so $g(\zeta) = \dots + b_3\zeta^{-3} + b_1\zeta^{-1} + a_1\zeta + a_3\zeta^3 + \dots$, where a_i and b_i are constants. Since the point $\zeta = 0$ maps to a finite point on $\Gamma(t)$, it follows that $b_i = 0 \forall i$. Further, requiring that the map be univalent implies $a_i = 0 \forall i \geq 3$. Since $\Im(z/\sqrt{2t}) \rightarrow \pm 1$ as $z \rightarrow \infty$ or, equivalently, $\zeta \rightarrow \pm 1$ it follows $a_1 = 1$. Thus, $g(\zeta) = \zeta$, so the map (12) takes the form

$$\frac{z}{\sqrt{2t}} = C + \frac{\zeta}{\pi} \log \left(\frac{\zeta - 1}{\zeta + 1} \right), \quad (13)$$

and it remains to determine C which is clearly real by symmetry. Now $\zeta \rightarrow \infty$ maps to the point $z = 0$ and locally the map must behave like $z \sim \zeta^{-2}$ in this limit. Expanding (13) for large ζ gives $C = 2/\pi$ and, finally, the map (5).

B Context of Valleys in Figures 7 and 9

In Figure 12, we show the contexts of valley heads from Figure 7 and Figure 9 within the network. The tendency of the heads from Figure 7 to be long and have at most small regions that are above threshold of motion suggests that these indeed represent diffusive, end-member valleys. The valley from Figure 9 is shorter with a greater proportion of area above the angle of repose, which suggests that this valley is growing faster.

C Mathematical Remarks

At the head of the valley ($y = 0$), the valley height $h(x, t)$ is given by

$$\frac{\pi x}{\sqrt{8t}} = 1 - \frac{\pi h}{2} \cot \left(\frac{\pi h}{2} \right), \quad (14)$$

for $0 < x/\sqrt{2t} < 2/\pi$. Since $2/\pi < 1$ the valley is steeper at its front compared to far downstream, and for $x \ll \sqrt{2t}$, (14) gives the local shape of the valley as $h \sim x^{1/2}$.

The free boundary problem (3) is, after suitable transformation, mathematically equivalent to that considered by Howison [20] and Howison and King [21] for the coating of a

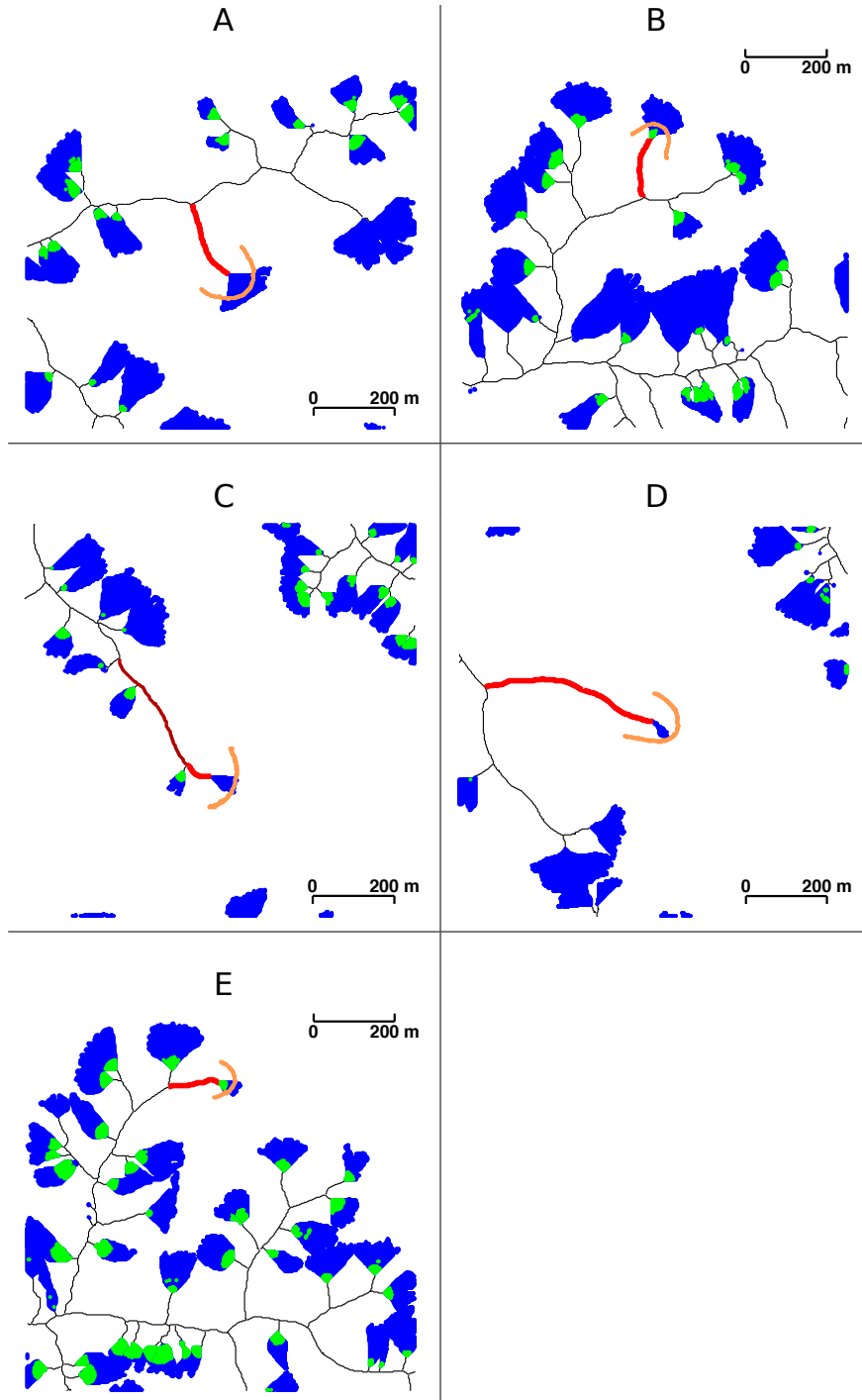


Figure 12: The locations within the network for the valleys shown in Figure 7. As in Figure 7, the contributing area is shown in blue calculated through a flow accumulation model [17], and regions above the angle of repose are shown in green. The first-order channel is indicated in red. The second-order channel for valley C is coloured a darker red to suggest that this channel may also be considered long and isolated. The orange contours indicate the location of the outermost contour of the fits in Figure 7.

semi-infinite plate by a viscous fluid. To see this, consider the Baiocchi transformation [22]: define the real function Ψ , the Schwarz potential, by

$$\Psi = \frac{z\bar{z}}{4} - \frac{1}{4} \int^z g dz - \frac{1}{4} \overline{\int^z g dz}, \quad (15)$$

where $g(z, t)$ is the Schwarz function of the boundary of Ω , i.e. $g(z, t) = \bar{z}$ on it. Note that (15) gives $\nabla^2 \Psi = 1$ in Ω and $\Psi_z = \Psi_{\bar{z}} = 0$ on the boundary, which, in turn, implies $\Psi = \partial\Psi/\partial n = 0$ on it. Also, $\dot{\Psi} = -p(x, y)$ (see e.g. Cummings et al. [22]) where $p = h(x, y) - 1$, and it follows that Ψ satisfies the free boundary problem

$$\begin{aligned} \nabla^2 \Psi &= 1, & \text{in } \Omega(t), \\ \Psi &= 0 \quad \text{and} \quad \partial\Psi/\partial n = 0 & \text{on } \Gamma, \\ \Psi &= t & \text{on } \gamma. \end{aligned} \quad (16)$$

Howison [20] uses potential plane methods to derive the map (5) to solve (16) and obtain the free boundary shape (8). Howison & King [21] later used the alternative method of Polubarinova-Kochina [23] to solve (16).